

LA-UR-11-4997

*Approved for public release;  
distribution is unlimited.*

*Title:* Simulating the Dynamics of Wind Turbine Blades:  
Part II, Model Validation and Uncertainty Quantification

*(Manuscript)*

*Author(s):* Kendra L. Van Buren, Clemson University  
Mark G. Mollineaux, Stanford University  
François M. Hemez, Los Alamos National Laboratory  
Sezer Atamturktur, Clemson University

*Intended for:* Wind Energy, August 2011



Los Alamos National Laboratory, an affirmative action/equal opportunity employer, is operated by the Los Alamos National Security, LLC for the National Nuclear Security Administration of the U.S. Department of Energy under contract DE-AC52-06NA25396. By acceptance of this article, the publisher recognizes that the U.S. Government retains a nonexclusive, royalty-free license to publish or reproduce the published form of this contribution, or to allow others to do so, for U.S. Government purposes. Los Alamos National Laboratory requests that the publisher identify this article as work performed under the auspices of the U.S. Department of Energy. Los Alamos National Laboratory strongly supports academic freedom and a researcher's right to publish; as an institution, however, the Laboratory does not endorse the viewpoint of a publication or guarantee its technical correctness.

## RESEARCH ARTICLE

## Simulating the dynamics of wind turbine blades: part II, model validation and uncertainty quantification

Kendra L. Van Buren<sup>1</sup>, Mark G. Mollineaux<sup>2</sup>, François M. Hemez<sup>3</sup> and Sezer Atamturkur<sup>1</sup>

<sup>1</sup> Department of Civil Engineering, Clemson University, Lowry Hall, Box 340911, Clemson, South Carolina 29634-0911, USA

<sup>2</sup> Department of Civil and Environmental Engineering, Stanford University, 473 Via Ortega, Room 314, Mail Code 4020, Stanford, California 94305, USA

<sup>3</sup> Los Alamos National Laboratory, XTD-Division (XTD-3), Mail Stop T087, Los Alamos, New Mexico 87545, USA

### ABSTRACT

Verification and validation (V&V) offers the potential to play an indispensable role in the development of credible models for the simulation of wind turbines. This paper highlights the development of a three-dimensional finite element model of the CX-100 wind turbine blade. The scientific hypothesis that we wish to confirm by applying V&V activities is that it is possible to develop a fast-running model capable of predicting the low-order vibration dynamics with sufficient accuracy. A computationally efficient model is achieved by segmenting the geometry of the blade into six sections only. It is further assumed that each cross section can be homogenized with isotropic material properties. The main objectives of V&V activities deployed are to, first, assess the extent to which these assumptions are justified and, second, to quantify the resulting prediction uncertainty. Designs of computer experiments are analyzed to understand the effects of parameter uncertainty and identify the significant sensitivities. A calibration of model parameters to natural frequencies predicted by the simplified model is performed in two steps with the use of, first, a free–free configuration of the blade and, second, a fixed–free configuration. This two-step approach is convenient to decouple the material properties from parameters of the model that describe the boundary condition. Here, calibration is not formulated as an optimization problem. Instead, it is viewed as a problem of inference uncertainty quantification where measurements are used to learn the uncertainty of model parameters. Gaussian process models, statistical tests and Markov chain Monte Carlo sampling are combined to explore the (true but unknown) joint probability distribution of parameters that, when sampled, produces bounds of prediction uncertainty that are consistent with the experimental variability. An independent validation assessment follows the calibration and is applied to mode shape vectors. Despite the identification of isolated issues with the simulation code and model developed, the overarching conclusion is that the modeling strategy is sound and leads to an accurate-enough, fast-running simulation of blade dynamics. This publication is Part II of a two-part effort that highlights the V&V steps required to develop a robust model of a wind turbine blade, where Part I emphasizes code verification and the quantification of numerical uncertainty. *Approved for unlimited public release on August 26, 2011, LA-UR-11-4997*. Copyright © 2012 John Wiley & Sons, Ltd.

### KEYWORDS

verification and validation; Bayesian inference; uncertainty quantification; sensitivity analysis; test–analysis correlation

### Correspondence

Kendra L. Van Buren, Department of Civil Engineering, Clemson University, Lowry Hall, Box 340911, Clemson, South Carolina 29634-0911, USA.

E-mail: klvan@clemson.edu

Received 8 September 2011; Revised 16 April 2012; Accepted 19 April 2012

## 1. INTRODUCTION

Wind energy research is being pursued in the USA as a viable alternative to provide a major amount of installed electrical power, as part of the ‘20% by 2030’ initiative by the US Department of Energy.<sup>1</sup> However, for wind energy to become a mainstay of energy needs, its cost must first be reduced drastically. The blades are responsible for only 10–15% of the cost of the wind turbine system;<sup>2</sup> however, damage to the blades can result in rotor instability that leads to damage of the entire wind turbine system.<sup>3,4</sup> To efficiently design for the next generation of wind turbines, it is crucial to understand the

dynamics of wind turbine blades, which capture all of the kinetic energy transported by the surrounding flow of wind, and improve the reliability of power generation from wind plants.<sup>5</sup> Better understanding of the wind turbine blades is essential, since the blades carry most of the structural loads that become imparted on the entire wind turbine. Better models would make more accurate predictions of performance, which would mitigate the operation and maintenance expenses associated with wind energy. These expenses currently start as low as \$5/MWh but climb to costs as high as \$20/MWh over a 20 year evolution of service.<sup>6</sup>

Modeling and simulation (M&S) offers a quicker, safer and more economical alternative to the conventional cycle of designing, prototyping and testing to study wind turbine blade behavior.<sup>7</sup> The versatility of modeling can be used to predict the response to many complex load cases,<sup>8</sup> but only idealized loads can usually be implemented in full-scale experiments.<sup>9</sup> In addition, parametric studies of damage to wind turbine blades can be investigated in an economical way through M&S, whereas the feasibility of such experimental campaigns would be limited because of the cost and safety implications.

Because of demands for faster turn-around times and the, sometimes, limited access to computing resources, there is a growing need to develop simplified 'engineering' models that can keep parametric and calibration studies to a manageable size.<sup>10</sup> It is also expensive, both in terms of memory management and time to solution, to couple a computational fluid dynamics (CFD) code to flexible dynamics models of the blades and, potentially, models of structural damage, to develop credible simulations of entire wind plants.<sup>11</sup> One approach to reduce this computational burden is to simplify the flexible dynamics of the wind turbine blade to speed up the calculations without, to the extent possible, sacrificing the prediction accuracy. The study presented in this paper, together with a companion publication, demonstrates the application of verification and validation (V&V) technology to achieve these goals.<sup>12</sup>

Our objective is to **develop a structural model that, while simplified as much as possible, still captures the dynamics of interest.** The V&V activities deployed in the companion paper (Mollineaux *et al.*<sup>12</sup>) and in this paper support essential steps of the model development process to guarantee that the simplifications introduced are justified for the intended purpose. V&V also serves the purpose of quantifying the experimental variability and numerical uncertainty (discussed in Mollineaux *et al.*<sup>12</sup>) and the model parameter uncertainty (discussed in this paper).

As explained in Mollineaux *et al.*<sup>12</sup>, the structure investigated is the 9 m, all-composite CX-100 blade designed at the Sandia National Laboratories. The finite element (FE) software is ANSYS version 12.1. The simplified model is developed on the basis of an as-accurate-as-possible description of the geometry obtained from design specifications. However, implementation of the materials relies on a strong assumption: the cross-sectional areas for the blade are modeled as smeared and isotropic material properties instead of modeling the multiple composite layers embedded in the epoxy matrix. The overarching goal of this effort is to demonstrate the extent to which V&V can be integrated to the model development of a **simplified yet validated** FE model, which delivers an acceptable level of predictive capability. Validated models that satisfy given time-to-solution requirements for the application of interest provide a competitive advantage.

Developing a predictive capability motivates the need to quantify the uncertainty introduced by assumptions imposed during the development of an FE model. Understanding the approximate behavior of a model renders it imperative to take into consideration *all* sources of uncertainty, as discussed in Section 2. Section 3 provides a cursory overview of the FE model of the CX-100 blade. (See Mollineaux *et al.*<sup>12</sup> for an in-depth discussion.) Section 4 discusses three V&V activities: the propagation of uncertainty from input parameters of the FE model to output predictions, sensitivity analysis and effect screening, and model calibration. These investigations are applied to low-order resonant frequencies of the blade according to a two-step approach. The response of the free–free model, followed by the fixed–free model, is evaluated, in an effort to decouple our understanding of material properties from that of model parameters that represent the boundary condition compliance. Section 5 presents an independent validation assessment on the basis of the ability of the calibrated model to correlate predicted and measured mode shape deflections. The implications and limitations of this study are discussed in Section 6.

## 2. REVIEW OF PERTINENT LITERATURE

Assumptions and simplifications, which are emphasized to only be able to provide an approximation of reality, are regularly imposed in numerical models. For example, beam property extraction methods, which require low computational cost and can be used for fast-running calculations, have been developed.<sup>13</sup> However, one study attempting to model a wind turbine system found that neglecting the effect of damping produced predictions with low goodness of fit to the experimental data.<sup>14</sup> This study, along with similar observations from other disciplines, suggests that not accounting for the uncertainty introduced by the simplifications and modeling assumptions can have a degrading effect on the quality of model predictions.

Another consideration is the relationship between goodness of fit to test data and the predictive capability of a model. It can be shown that fidelity to data, robustness to assumptions and predictive capability are antagonistic attributes of any family of models.<sup>15</sup> This can be described using the case of over-fitting, which happens when a model produces accurate predictions for configurations to which it was calibrated. But this may come at the cost of reducing its predictive capability, that is, the accuracy of its predictions when attempting to simulate other, non-tested configurations. Understanding these

trade-offs is important for the development of robust CFD and FE models because it is important that models are robust to sources of variability, such as the significant variability between wind turbine blades that will result in different levels of structural response.<sup>16</sup>

It is also important to account for the uncertainty associated with experimental procedures. The vibration testing of an article in a free–free configuration can often be affected by the positioning of the straps, mass loading of the accelerometers and orientation of the test specimen.<sup>16,17</sup> The free–free boundary condition is, on the other hand, trivial to simulate numerically. When free–free is not an option, proper modeling of the boundary condition becomes necessary to ensure that the predictions of structural response can be compared with measurements. Modeling a fixed–free boundary condition is a possibility, as long as the non-ideal compliance of the attachment setup can be accounted for, if it is believed important to do so. An unknown, boundary compliance can also significantly influence what is observed during a vibration test. To mitigate the uncertainty associated with a fixed-boundary compliance, studies originating at Sandia National Laboratories propose a new setup for the modal analysis of wind turbine blades, in which a 9 m blade is mounted vertically on a seismic mass and airbag system.<sup>10,18</sup> This type of boundary condition is designed so that its characteristics would be well characterized and modeled accurately in the simulation of the structural model. The setup assures that the fixity of the blade to the seismic mass is rigid and that there is a soft boundary condition when placed on the airbags, which can be characterized by stiffness properties. In a further investigation of boundary condition effects, the experimental modal analysis of a stationary wind turbine system is performed.<sup>19</sup> Blade and tower responses to impact hammer testing are characterized. The mode shapes identified during these vibration tests demonstrate that there is significant coupling between the different blades and tower, confirming that the tower of a wind turbine system does not behave as a rigid body.

Recently, the development of FE models has gained acceptance for routine use in the study of wind turbine blades. Another common practice is to perform calibration against experimental data as an integral part of model development. The work by Bechly and Clausen<sup>20</sup> provides an early attempt to utilize FE modeling in the design and analysis of wind turbine blades by using shell and solid elements. The study researched the optimal design of a 2.5 m long blade, and experimental data from fabricated blades were analyzed to validate predictions of the FE model. Another early attempt used free–free modal data collected from a 4 m section of a blade to calibrate an FE model.<sup>21</sup> Accuracy was improved by collecting additional measurements of the geometry of the blade and increasing the resolution of the simulation (higher mesh density). It was found that, with the use of these approaches, the number of assumptions needed to model the blade section could be reduced. Other studies have since investigated the use of M&S to study the behavior of wind turbine blades, owing to the versatility of numerical models.<sup>22,23</sup> The current study builds on previous research efforts to model wind turbine blades and places an emphasis on the use of V&V activities to establish the predictive capability of numerical simulations.

### 3. DEVELOPMENT OF THE SIMPLIFIED FE MODEL

This section provides a cursory overview of the FE model of the CX-100 blade. The reader is referred to Mollineaux *et al.*<sup>12</sup> for details about the model development and quantification of solution (or numerical) uncertainty. The brief explanation provided here is useful to better understand the uncertainty quantification, sensitivity analysis and calibration steps discussed in Section 4.

The model of the CX-100 wind turbine blade is developed with the NuMAD pre-processor and imported into the ANSYS software. The blade is 9 m long, and its geometry is imported from another, high-fidelity FE model with as few simplifications as possible. Solution verification, which utilizes the results of a mesh refinement study, is performed, to quantify the overall level of numerical uncertainty due to mesh discretization. A discretization based on an element size of  $\Delta x = 8$  cm is deemed appropriate because it provides an overall solution uncertainty of 1.78%. This is comparable with the maximum level of experimental variability obtained by replicating the modal tests, where the  $\pm 3\sigma$  bounds of uncertainty are estimated to be 1.62%. The other criterion adopted to select the level of resolution is to be able to perform a modal extraction in less than 60 s on a PC-based computing platform (Intel single-core, 2 GHz processor, 4 GB memory, Windows 7 operating system), which is a constraint that needs to be met in order to make parametric studies feasible. (See Mollineaux *et al.*<sup>20</sup> for details.) The mesh arrived at counts 3070 elements and computes the modal solution in less than 60 s.

To simplify the parameterization of the model, only six independent sections are defined, compared with high-fidelity models that require hundreds of sections. Most of them are illustrated in Figure 1. They are the shear web, root, spar cap, trailing edge, leading edge with balsa and leading edge without balsa. The shear web runs along most of the length of the blade, and it is not shown in the figure because of its location on the inside. Within each one of these sections, an isotropic material is defined with smeared cross-sectional properties. The validity of this assumption is explored in Section 4 to assess the credibility of the simulation.

Modal testing of the CX-100 wind turbine blade is carried out under free–free and fixed–free boundary conditions at the Los Alamos National Laboratory.<sup>12,17</sup> Roving impact hammer tests are performed to amass modal data at three locations with uniaxial accelerometers. A linear average is used with five repeats and a 150 Hz sampling frequency. The acceleration

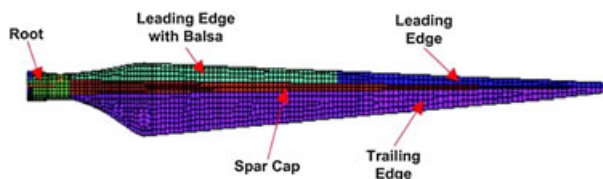


Figure 1. Illustration of the ANSYS model showing different sections of the blade.

Table I. System identification of the CX-100 blade with free–free modal testing.

Type of mode	Mean statistic (Hz)	Standard deviation (Hz)	Variability <sup>a</sup> (%)
First flapwise bending	7.617	0.004	0.06
Second flapwise bending	20.167	0.055	0.27
Third flapwise bending	32.256	0.051	0.16

<sup>a</sup>The coefficient of variance is defined as the standard deviation divided by the mean. It is based on 27 replicates for free–free vibration testing.

Table II. System identification of the CX-100 blade with fixed–free modal testing.

Type of mode	Mean statistic (Hz)	Standard deviation (Hz)	Variability <sup>a</sup> (%)
First flapwise bending	3.221	0.008	0.24
Second flapwise bending	8.824	0.011	0.12
Third flapwise bending	19.204	0.020	0.11

<sup>a</sup>The coefficient of variance is defined as the standard deviation divided by the mean. It is based on 27 replicates for fixed–free vibration testing.

response is measured for 11 s, during which the response of the blade is attenuated. This procedure negates the use of a window function. The levels of experimental variability are quantified and listed in Tables I and II for the free–free and fixed–free boundary conditions. The observed variability is attributed to potential calibration errors, operator-to-operator variability and the inability to identically repeat the experiments on the same test specimen of the CX-100 blade. The fact that it does not account for any specimen-to-specimen or test setup variability explains the overall low levels of uncertainty observed during this campaign of vibration testing.

## 4. PROPAGATION OF UNCERTAINTY, SENSITIVITY ANALYSIS AND CALIBRATION

Section 4 presents results of the V&V study. The discussion starts by formulating questions about specific aspects of the predictive capability being developed. The main contribution of this publication is to demonstrate how V&V activities, such as mesh refinement or effect screening, can be integrated to model development to start answering those questions. Simulations are analyzed first for free–free vibrations of the CX-100 blade (Sections 4.2 and 4.3). The fixed–free configuration is analyzed next to decouple the parameterization of the boundary condition from the description of homogenized material properties in the model (Sections 4.4 and 4.5).

### 4.1. Specific questions about the predictive capability

We would like to answer the following four questions regarding specific aspects of the predictive capability provided by the fast-running engineering model of the CX-100 blade.

- **Question A:** What is an appropriate level of mesh resolution for the calculations?
- **Question B:** What are the mechanisms that most influence the variability of predictions?
- **Question C:** Can measurements be used to reduce parametric uncertainty in the model?
- **Question D:** Does the model provide accurate-enough predictions of mode shapes?

Question A is answered in Mollineaux *et al.*<sup>12</sup> where it is shown how a mesh refinement study can be combined to an upper-bound estimate of solution uncertainty. It is found, as noted in Section 3, that a discretization of  $\Delta x = 8$  cm leads to an overall solution uncertainty of 1.78%. Running the modal analysis at this level of resolution provides a time to solution of 60 s, approximately, which is fast enough to enable parametric studies with thousands of runs.

Question B promotes understanding of what controls the prediction variability. By learning which parameters are most influential to explain how the predictions change, one can control them in order to reduce the prediction uncertainty. It is equally important to learn which parameters do not control the prediction uncertainty because attempting to better control a non-influential effect would be both inefficient and a waste of important resources. The prediction variability observed from a design of experiments (DOE) is decomposed into separate effects to answer Question B.

Recall that the model is parameterized into only six sections and that each section is described by homogenized material properties. The resulting idealization is anything but high fidelity since the real structure involves a multi-layered composite material. Our point of view is that there is no such thing as ‘true’ values of these material properties. What becomes essential is to reduce as much as possible the initially large lack of knowledge of these fictitious parameters, which is the subject of Question C. The vibration measurements are used to search for values that, while they remain uncertain, lead to predictions that better match the experimental data.

Finally, Question D exemplifies the validation assessment. Whereas the propagation of uncertainty, sensitivity analysis and calibration are applied to frequency predictions, validity of the simplified model is assessed using mode shape predictions. The rationale is to investigate predictions that have not been exploited for calibration, hence promoting the use of separate datasets between development and validation of the model. Another reason for this choice is that accurate predictions of mode shape deflections are important to couple the structural dynamics and CFD-based simulation of flow around the turbine. It may, arguably, be even more important than predicting the resonant frequencies accurately. Question D is answered through conventional test–analysis correlation (TAC).

## 4.2. Propagation of uncertainty and sensitivity analysis of the free–free configuration

As noted previously, it is important to assess what controls the prediction variability. Understanding which parameters, or groups of parameters, are most influential allows for the elimination of the insensitive ones. It promotes computational savings and a more efficient calibration.

Following the mesh discretization studied in Mollineaux *et al.*<sup>12</sup>, the next dominant lack of knowledge in the problem comes from the idealization of the composite material as uniform and isotropic. Material properties (modulus of elasticity,  $E$ , and density,  $\rho$ ) are approximated using the rule of mixtures for composites, which provides ranges  $[E_{\text{Min}}; E_{\text{Max}}]$  and  $[\rho_{\text{Min}}; \rho_{\text{Max}}]$  for each parameter.<sup>24</sup> To simulate the free–free vibrations, the model is parameterized using a total of 12 parameters, which are the modulus of elasticity ( $E$ ) and density ( $\rho$ ) for the six sections of the blade.

The first step of the analysis is to propagate uncertainty from the 12 parameters to resonant frequency predictions. A two-level, full-factorial DOE is used, whereby all combinations of lower and upper bounds for the 12 parameters are executed. The design results in a total of  $2^{12} = 4096$  evaluations of the FE model. Figure 2 compares predictions from these 4096 runs to the mean statistic of measured frequencies for the first mode. The fact that measurements fall within the range of frequencies predicted by the DOE is confirmation that the model captures the first flapwise bending reasonably well. However, the prediction uncertainty obtained by propagating the initial ranges of 12 parameters is quite significant relative to the experimental variability. (Recall  $\sigma = 0.004$  Hz only from Table I.)

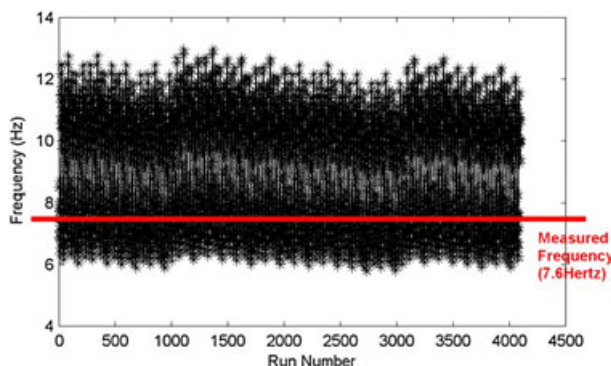


Figure 2. Comparison of first-mode simulation uncertainty and measured frequency.

The second step is to understand which parameters, or combinations of parameters, cause the large uncertainty illustrated in Figure 2. Our hypothesis is that only a few parameters, out of the 12 considered, are statistically significant to explain how the predictions vary. Two additional DOEs are analyzed to confirm, or refute, this hypothesis. A Latin hypercube sample with 1000 runs is analyzed first to identify the potentially non-significant parameters.<sup>25</sup> From an analysis of variance (ANOVA), the number of significant parameters is reduced from 12 to 8.<sup>26</sup> This first design is supplemented by the analysis of a two-level, full-factorial DOE that requires another  $2^8 = 256$  runs, to further screen the significant parameters down to five only.

A tool that originated from high-consequence studies on nuclear reactor safety, known as the Phenomenon Identification and Ranking Table (PIRT), is used to screen the parameters.<sup>27</sup> The PIRT provided in Table III organizes results obtained with the two-level, full-factorial design. The average variability of frequency predictions for the first three flapwise bending modes is analyzed using a main-effect ANOVA. ‘Main effect’ means that the study is restricted to the influence of varying one parameter at a time, without considering potential interactions or higher-order effects. Large values of the  $R^2$  composite statistics listed in Table III identify the most significant main effects.

Because the 12 parameters considered are unknown, the uncertainty column of the PIRT is omitted in Table III. The lower and upper bounds listed indicate the ranges exercised in the full-factorial design. Values of the main-effect  $R^2$  statistics are scaled to 100%. The PIRT indicates that five of the 12 parameters control nearly 95% of the main-effect variability of frequency predictions. These five parameters are kept for further study, whereas the others are eliminated. The two DOEs—(i) the two-level, full-factorial design with 12 parameters and (ii) the Latin hypercube sample design with 12 parameters, then two-level, full-factorial design with eight parameters—arrive at the same list of five most influential parameters. This comparison between two approaches provides evidence that the statistically most significant parameters are identified and that this result is independent of how the screening is performed.

After the initial 12 parameters are screened, an initial TAC of mode shapes is performed to ensure that (i) the experimental and numerical mode shapes are paired appropriately and (ii) mode swapping does not occur as the material properties are perturbed. A two-level, full-factorial DOE is analyzed to exercise all combinations of lower and upper bounds for the five influential parameters identified in Table III. The mode shape deflections are obtained for these  $2^5 = 32$  combinations and plotted in Figure 3. Although varying the model parameters between the lower and upper bounds

**Table III.** PIRT developed for main-effect screening of 12 FE model parameters.

Factor	Description	Lower bound	Upper bound	$R^2$ values	Keep?
A	Shear web, $\rho$	650.46 kg m <sup>-3</sup>	1084.10 kg m <sup>-3</sup>	0.29%	No
B	Root, $\rho$	2071.56 kg m <sup>-3</sup>	3452.60 kg m <sup>-3</sup>	0.37%	No
C	Lower-edge balsa, $\rho$	1025.05 kg m <sup>-3</sup>	1708.42 kg m <sup>-3</sup>	0.32%	No
D	Spar cap, $\rho$	1900.44 kg m <sup>-3</sup>	3167.40 kg m <sup>-3</sup>	1.11%	No
E	Trailing edge, $\rho$	411.90 kg m <sup>-3</sup>	686.50 kg m <sup>-3</sup>	9.35%	Yes
F	Leading edge, $\rho$	1287.30 kg m <sup>-3</sup>	2145.50 kg m <sup>-3</sup>	3.03%	Yes
G	Shear web, $E$	0.99 MPa	2.97 MPa	1.74%	No
H	Root, $E$	18.01 MPa	54.02 MPa	0.00%	No
I	Lower-edge balsa, $E$	4.36 MPa	13.08 MPa	1.74%	No
J	Spar cap, $E$	31.04 MPa	93.12 MPa	65.95%	Yes
K	Trailing edge, $E$	0.92 MPa	2.75 MPa	9.85%	Yes
L	Leading edge, $E$	10.30 MPa	30.91 MPa	6.25%	Yes

Column 5 lists composite  $R^2$  statistics obtained for main-effect analysis by averaging individual  $R^2$  for predictions of resonant frequencies of the first three flapwise bending modes (modes 1, 3 and 4).

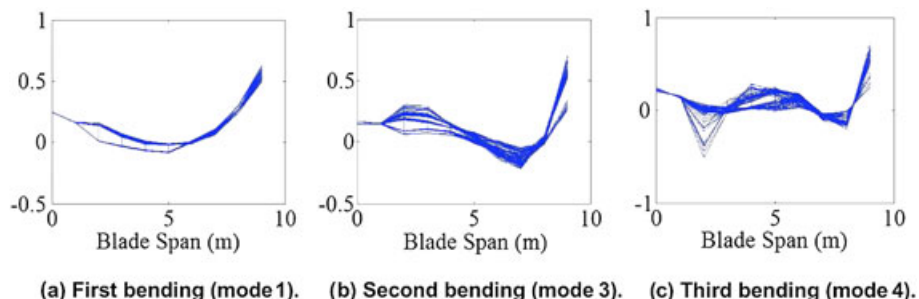


**Figure 3.** TAC of mode shape deflections used for the five-parameter study.

**Table IV.**  $R^2$  statistics for total-effect analysis of five parameters of the FE model.

FE model parameter	Parameter lower bound	Parameter upper bound	$R^2$ statistics of total effect		
			Mode 1	Mode 3	Mode 4
Trailing edge, $\rho$	411.90 kg m <sup>-3</sup>	686.50 kg m <sup>-3</sup>	3.46%	10.15%	15.95%
Leading edge, $\rho$	1287.30 kg m <sup>-3</sup>	2145.50 kg m <sup>-3</sup>	4.63%	9.68%	7.47%
Spar cap, $E$	31.04 MPa	93.12 MPa	28.57%	28.50%	42.44%
Trailing edge, $E$	0.92 MPa	2.75 MPa	0.08%	6.39%	2.18%
Leading edge, $E$	10.30 MPa	30.91 MPa	12.58%	32.69%	28.90%

generates significant mode shape variability, these shapes consistently correspond to the flapping deflection, and mode swapping does not occur because of parameter variations.

With a confirmation that the modal pairing is unchanged within the ranges of variation of the five most influential parameters, a three-level, full factorial DOE is analyzed on the basis of  $3^5 = 243$  runs. Each parameter is set to a lower bound, nominal value (mid-range) or an upper bound as listed in Table IV. Three levels are used such that the main effects, linear interactions and quadratic effects can all be captured without significant statistical aliasing. This last design generates the training data needed to develop a fast-running, statistical emulator for each resonant frequency.

A final sensitivity analysis is performed using the training data, with results given in Table IV. The table lists the total-influence ANOVA statistics for each bending frequency considered. The total effect includes the main effect and all higher-order interactions that involve a given parameter. This analysis confirms that all the parameters kept exercise some degree of influence on the first three flapwise bending modes of the CX-100 blade model.

### 4.3. Inference uncertainty quantification of the free-free configuration

At this point, uncertainty has been propagated forward through the simulation of blade vibration and the important parameters that control the prediction variability have been learned. This answers Question B of Section 4.1. Even though the main sources of uncertainty have been reduced to five material properties, acceptable ranges for these parameters remain largely unknown. The next step addresses Question C by attempting to reduce this lack of knowledge. Vibration measurements of the free-free configuration are used to explore settings of the homogenized material properties that lead to predictions that better match the experimental data.

This question could be formulated as a deterministic optimization that searches for the ‘best’ combination of the five material properties. Instead of a deterministic calibration, Question C is addressed through **inference uncertainty quantification**, which explores the posterior probability distribution of the five parameters. By definition, the posterior is the probability law that leads to predictions of resonant frequencies that are statistically consistent with the experimental data. The challenge is that the posterior function is unknown and must be explored using a Markov chain Monte Carlo (MCMC) algorithm, which turns out to be computationally expensive. Replacing the FE model by fast-running, statistical emulators developed with Gaussian process models (GPMs) alleviates this difficulty. A GPM is simply a probability distribution whose hyper-parameters, such as mean value and correlation structure, have been trained using the 243 simulation runs of Section 4.2. Predictions are then obtained by sampling the probability law instead of analyzing the computationally expensive FE model.

In the absence of qualitative data about the material, a uniform prior distribution is assumed in the formulation of the GPM. The computational procedure exercised in this study relies on a methodology first proposed in a univariate formulation and later expanded into the multivariate formulation.<sup>28,29</sup>

Table V summarizes the inference results. Columns 2–4 summarize the prior uncertainty, that is, the ranges within which the five material properties are varied in the full-factorial design. This is prior to any comparison between numerical

**Table V.** Comparison of prior and posterior uncertainty of five FE model parameters.

Input factor	FE model parameter	Prior uncertainty			Posterior uncertainty		
		Lower	Upper	Range	Mean	Standard deviation	$\pm 2\sigma$ range
E	Trailing edge, $\rho$ (kg m <sup>-3</sup> )	411.90	686.50	274.60	607.09	61.36	245.44
F	Leading edge, $\rho$ (kg m <sup>-3</sup> )	1287.30	2145.50	858.20	1703.90	246.03	984.13
J	Spar cap, $E$ (MPa)	31.04	93.12	62.08	41.74	5.91	23.64
K	Trailing edge, $E$ (MPa)	0.92	2.75	1.83	1.92	0.22	0.88
L	Leading edge, $E$ (MPa)	10.30	30.91	20.61	19.54	5.75	23.00

predictions and physical measurements. Columns 5–7 describe the posterior uncertainty, that is, the statistics inferred by performing 100,000 trials of the MCMC search algorithm. Each trial consists in evaluating a new combination of the five parameters by comparing GPM predictions of the three frequencies to measurements. The model visited is retained only if its predictions pass a statistical test of goodness of fit with the experimental data and variability. After the MCMC iterations are completed, the posterior probability law is inferred from the empirical distribution of the most often visited models. These models are those that predict resonant frequencies in acceptable agreement with the measurements. This is assessed using a goodness-of-fit metric that compares predictions and measurements. The MCMC sampling algorithm tends to gravitate around models that yield a better goodness of fit. Hence, the higher-probability parameter values correspond to models whose predictions match, on average, the measurements with higher accuracy.

Figure 4 illustrates graphically the five-dimensional posterior probability function corresponding to Table V. Each box on the main diagonal represents a marginal distribution for one of the five parameters. Each off-diagonal box depicts a probability contour for a pair of parameters.

The posterior bounds of  $\pm 2$  standard deviations listed in Table V (column 7) can be compared with the prior ranges (column 4). This uncertainty is reduced by, at least, twofold for the moduli of elasticity of the spar cap (factor J) and trailing edge (factor K). This is confirmed graphically by the narrow marginal histograms of these two parameters in Figure 4. Knowledge of the two parameters of the leading edge (factors F and L) is not improved significantly likely because, as shown in Table III, they contribute only 3% and 6%, respectively, to the overall variability in the model. This is illustrated in Figure 4 by relatively ‘flat’ histograms of sampled values, which indicate non-informative, posterior marginal functions.

Another important observation from the off-diagonal contours of bivariate probability is that there is no significant correlation between the five model parameters. Observing a correlation would invalidate the development of a simplified engineering model that is based on defining a small number of independent and uncorrelated sections of the blade. It would also generate trade-offs between parameter values that would make it difficult to calibrate the model. Results presented in Table V and Figure 4 answer Question C by demonstrating that it is possible, at least for two of the five parameters, to reduce the parametric uncertainty in the model through the combination of sensitivity analysis and parameter inference.

Figure 5 compares the mean statistics of vibration measurements (with blue dashed lines) to predictions obtained before and after inference uncertainty quantification. Samples from the prior ranges are shown with red dot symbols, whereas those of the posterior  $\pm 2\sigma$  bounds are shown with green star symbols. Each subplot corresponds to one of the frequencies of interest. The figure indicates that, as expected, combinations of parameters sampled from the joint, posterior distribution yield models whose predictions tend to agree better with measurements. It confirms that the inference, while reducing the uncertainty of three of the most influential parameters (see Table V), also contributes to better predictions of the flapwise vibration modes of interest.

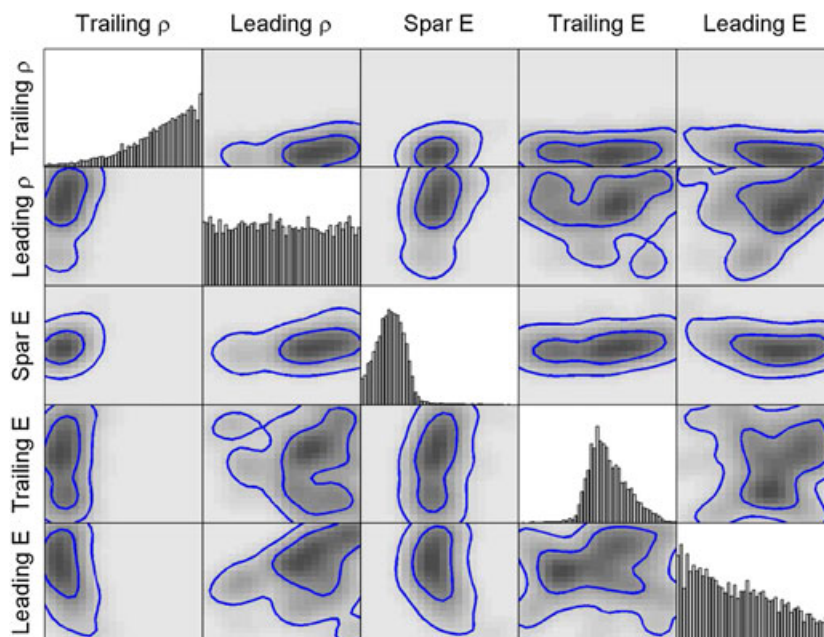
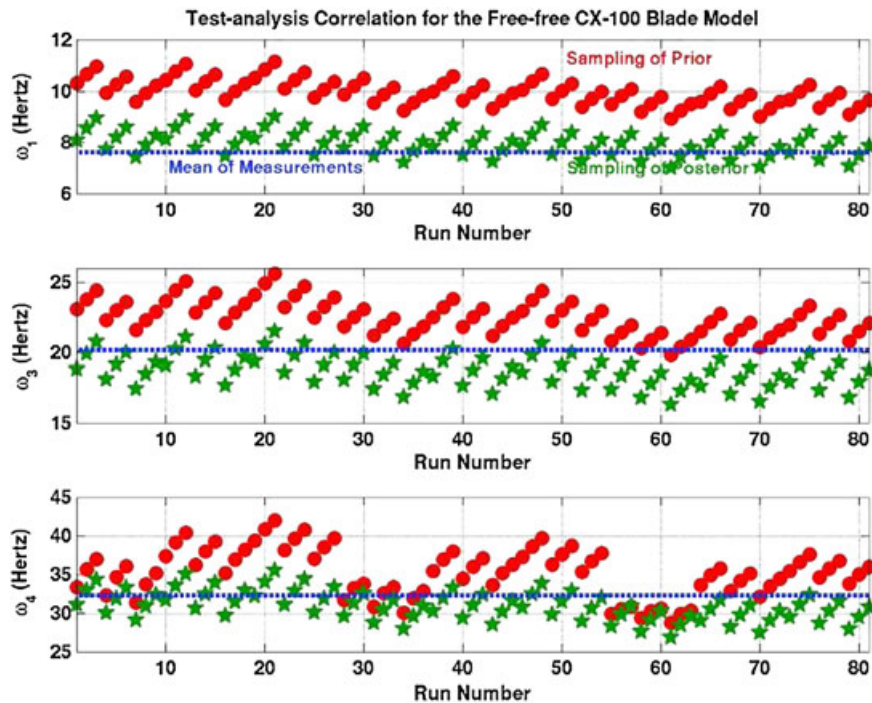


Figure 4. Marginal distribution and correlation functions corresponding to Table V.



**Figure 5.** Prior and posterior predictions for the free–free configuration.

The fixed–free configuration of the CX-100 blade is investigated next. The simplified model is essentially the same, with the exception of adding springs to the base to represent the boundary condition compliance. In this second stage, the sensitivity analysis and inference are focused on reducing the uncertainty of material properties for the root section and boundary springs.

#### 4.4. Propagation of uncertainty and sensitivity analysis of the fixed–free configuration

The analysis proceeds with the numerical simulation of the fixed–free configuration of the blade where additional springs are added to represent the boundary condition compliance. Separating the free–free and fixed–free configurations decouples the homogenized properties investigated so far in Sections 4.2 and 4.3 from those of the fictitious boundary springs.

Figure 6 shows that the fixed–free configuration is realized experimentally by attaching the CX-100 blade to a steel ‘bookend’ fixture, weighing approximately 500 lbf (or 250 kg). Although this attachment is used to create a fixed boundary condition, there is an inherent uncertainty due to the difficulty in producing an infinitely rigid connection. Fictitious springs are implemented in the simplified FE model to account for this uncertainty and generate a boundary condition for which the support is neither completely ‘free’ nor ‘fixed’. It is also noted, through an effect screening study, that rotational springs

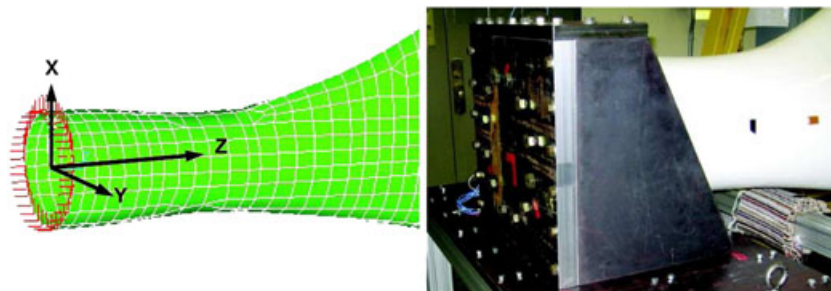


**Figure 6.** Close-up of the simulated springs (left) and close-up of the bookend (right).

at the base of the blade do not exercise any significant influence on the vibration characteristics. The fixture attachment is limited to translational springs that are added in the  $X$ ,  $Y$  and  $Z$  directions at 40 locations around the diameter of the base of the root. Springs in the  $X$  and  $Y$  directions are assumed to be identical because they act in the same plane.

A difficulty introduced by the addition of boundary springs is that parametric studies are prone to mode swapping as the spring stiffness coefficients are varied. As shown in Figure 7, a mismatch between the first modes of the simulated free-free and fixed-free configurations is observed. It is deduced from this comparison that the first flapwise bending mode of the fixed-free setting is not obtained until the boundary springs are sufficiently stiff. A preliminary parametric study is therefore devoted to learning ranges for the spring stiffness coefficients that, while they avoid mode swapping as much as possible, transition between the free-free and fixed-free conditions.

Simulations indicate that the vibration behavior converges asymptotically to the fixed-free blade when the boundary spring stiffness coefficients are sufficiently large. Likewise, decreasing the coefficients converges to the free-free behavior. This is illustrated in Figure 8. The first flapwise mode of the free-free configuration occurs for spring stiffness coefficients smaller than  $10^{+6} \text{ N m}^{-1}$ , approximately. The vibration behavior approaches the fixed-free configuration for coefficients that exceed  $10^{+8} \text{ N m}^{-1}$ . These two values are, therefore, good candidates to define the lower and upper bounds of the subsequent parametric studies.

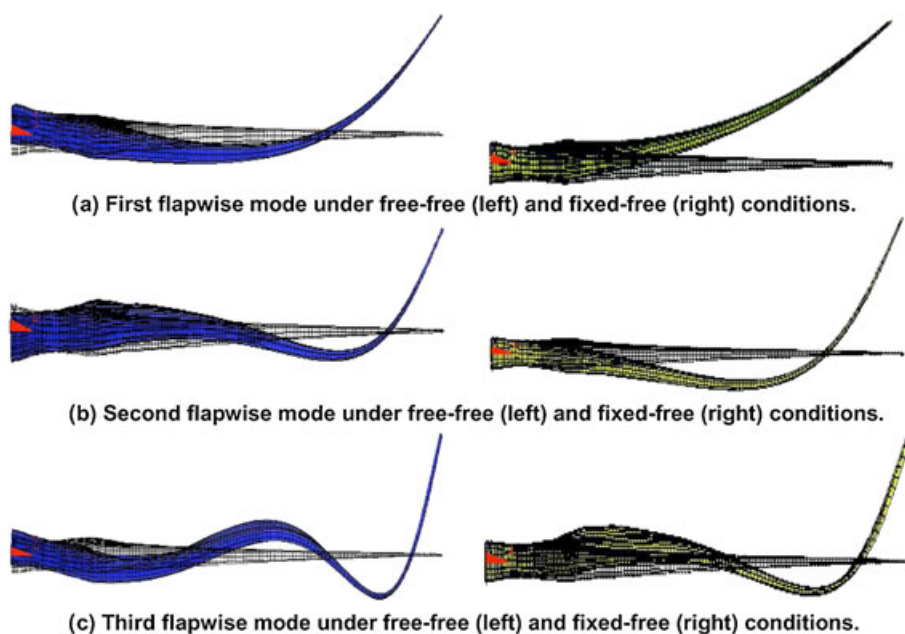


Figure 7. Comparison of the simulated free-free and fixed-free mode shape deflections.

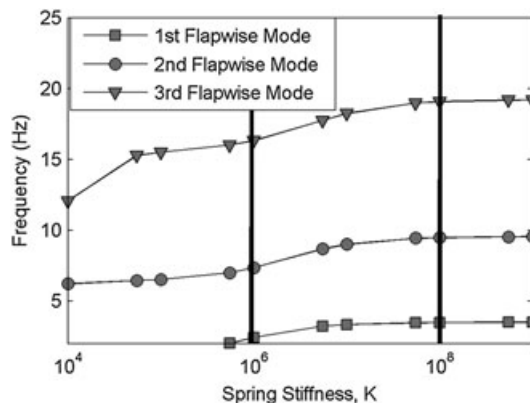


Figure 8. Effect of varying the boundary spring coefficients on bending frequencies.

The lower bound cannot be argued about because decreasing the boundary spring coefficient below  $10^{+6} \text{ N m}^{-1}$  suppresses the first free-free flapwise bending mode, as indicated in Figure 8. To verify that the upper bound yields a stiff-enough attachment, a comparison is made with a simulation where the boundary springs are removed and, instead, nodes at the base of the blade are fixed in all directions. Figure 9 compares the first three flapwise bending deflections of this pinned connection to those obtained with boundary spring coefficients of  $10^{+8} \text{ N m}^{-1}$ . The figure indicates an excellent agreement between the two sets of shapes. In addition, frequency differences do not exceed 0.1%. From these observations, it is concluded that setting the upper bound at  $10^{+8} \text{ N m}^{-1}$  suffices to define the fixed-free boundary condition.

Sensitivities of the simplified model for the fixed-free boundary condition are investigated next. It is noted that a complete analysis is unnecessary because the simplified model has already been studied in the free-free configuration. Only the homogenized material properties that are anticipated to exercise a statistically significant effect need to be re-evaluated. They include parameters for the spar cap (factor J) and trailing edge (factors E and K), according to Table III. In the free-free case, properties of the root were found to be insignificant contributors to the resonant frequency variability. In the fixed-free case, however, the strain energy is re-distributed and shifted towards the base of the blade. Therefore, the material parameters of the root section must be included in the study, together with the stiffness coefficients of boundary springs.

These considerations suggest a total of seven model parameters to investigate the variability of resonant frequencies and mode shape deflections. The seven parameters include one stiffness coefficient for boundary springs added in the Z direction and another stiffness coefficient for all springs parallel to either the X or Y axis. A two-level, full-factorial DOE is utilized in an attempt to keep the parametric study to a manageable size with  $2^7 = 128$  runs. A two-level design is deemed sufficient to screen the statistically significant effects.

Table VI summarizes the results of sensitivity analysis by listing the total-effect  $R^2$  statistics from the decomposition of variability for the first three flapwise bending frequencies. The material properties of the root section (factors B and H) are observed to have an insignificant effect on the vibration response of the model. It is possible that the more dominant parameters simply outweigh the contribution of these properties for the root section. It is also observed that only the translational springs in the Z direction have a significant influence on the response. This is likely because the flapwise bending behavior of the blade exercises the springs oriented in the Z direction, which are parallel to the orientation of the spar cap (see Figure 6). This bending does not strain springs oriented in the (X; Y) plane as much, which explains the low influence of parameter  $k_1$  in Table VI.

The sensitivity results are used to reduce the number of parameters from seven to three, as shown in Table VI. A four-level, full-factorial design, populated with  $4^3 = 64$  runs, is analyzed next to generate the training data required for inference in Section 4.5. The bounds within which each parameter is allowed to vary are those listed in Table VI. The objective of inference uncertainty quantification is to reduce this lack of knowledge as much as possible.

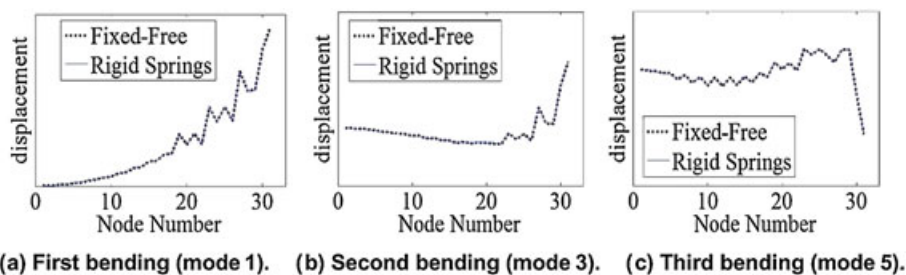


Figure 9. Shapes of a pinned boundary compared with those obtained with  $k = 10^8 \text{ N m}^{-1}$ .

Table VI. Total-effect  $R^2$  statistics for seven parameters of the fixed-free configuration.

Input factor	FE model parameter	Parameter lower bound	Parameter upper bound	Total-effect $R^2$ statistics			Keep?
				Mode 1	Mode 3	Mode 5	
B	Root, $\rho$	2072 $\text{kg m}^{-3}$	3453 $\text{kg m}^{-3}$	0.00%	0.00%	0.00%	No
E	Trailing edge, $\rho$	484.4 $\text{kg m}^{-3}$	729.8 $\text{kg m}^{-3}$	1.59%	5.14%	12.47%	Yes
H	Root, $E$	18.01 MPa	54.02 MPa	0.18%	0.58%	0.72%	No
J	Spar cap, $E$	29.92 MPa	53.56 MPa	6.90%	27.30%	29.17%	Yes
K	Trailing edge, $E$	1.48 MPa	2.35 MPa	0.07%	0.15%	5.17%	No
M	(X; Y) spring, $k_1$	$10^{+6} \text{ N m}^{-1}$	$10^{+8} \text{ N m}^{-1}$	0.00%	0.00%	0.03%	No
N	Z spring, $k_2$	$10^{+6} \text{ N m}^{-1}$	$10^{+8} \text{ N m}^{-1}$	39.44%	66.26%	50.14%	Yes

### 4.5. Inference uncertainty quantification of the fixed-free configuration

The results of inference uncertainty quantification are briefly summarized for simulations of the fixed-free configuration. The statistics of the MCMC exploration of the three-parameter space (factors E, J and N of Table VI) are listed in Table VII and posterior distributions are illustrated in Figure 10. These statistics are obtained with 20,000 iterations for the MCMC exploration of the three-parameter space. This number of samples is sufficient to estimate the posterior probability distribution with reasonable accuracy. This is because common practice is to use no fewer than a hundred iterations per variable explored, which would require about 300 samples for our application. Using 20,000 iterations exceeds this minimum expectation to provide sufficiently converged statistics.

Again, the inference successfully reduces the lack of knowledge of the modulus of elasticity of the spar cap (factor J). This does not come as a surprise because this factor is the second most influential. The reduction of uncertainty is indicated by a narrow histogram in Figure 10. It is also apparent that the statistics of the modulus of elasticity obtained with inference of the free-free configuration ( $E = 41.7 \pm 5.9$  MPa in Table V) are consistent with those obtained with inference of the fixed-free configuration ( $E = 40.7 \pm 2.8$  MPa in Table VII).

The inference is not able, on the other hand, to mitigate our ignorance of the boundary spring coefficient in the Z direction (factor N). Table VI shows that this failure cannot be attributed to a lack of sensitivity of resonant frequencies to the spring coefficient. A possible explanation is that the bookend attachment of the blade is not massive enough to facilitate the storage of a significant quantity of strain energy near the base. Consequently, the vibration measurements may be somewhat uninformative to constrain the value of the boundary spring stiffness. The inference is also unsuccessful for the density of the trailing edge (factor E). This could be due to a potential interaction between the density and the boundary spring during calibration. The contribution of the density to the overall variability of the model in both the free-free and fixed-free cases is low relative to the other parameters, possibly resulting in poor inference results.

Figure 11 is the counterpart of Figure 5 and shows a comparison between the mean statistics of vibration measurements (with blue dashed lines) and predictions of the simplified FE model obtained before and after inference. Samples from the prior ranges are shown with red dot symbols, whereas those of the posterior  $\pm 2\sigma$  bounds are shown with green star symbols. Each subplot corresponds to one of the frequencies of interest. It can be observed that, even though the study is restricted to three parameters only, samples obtained from the posterior distribution tend to agree better with the physical measurements.

**Table VII.** Comparison of prior and posterior uncertainty of three FE model parameters.

Input factor	FE model parameter	Prior uncertainty			Posterior uncertainty		
		Lower	Upper	Range	Mean	Standard deviation	$\pm 2\sigma$ range
E	Trailing edge, $\rho$ ( $\text{kg m}^{-3}$ )	484.37	729.81	245.44	593.11	66.99	267.96
J	Spar cap, $E$ (MPa)	29.92	53.56	23.64	40.66	2.76	11.04
N	Z spring, $k_2$ ( $\times 10^{+6}$ N m $^{-1}$ )	1.00	100.00	99.00	53.71	27.59	110.36

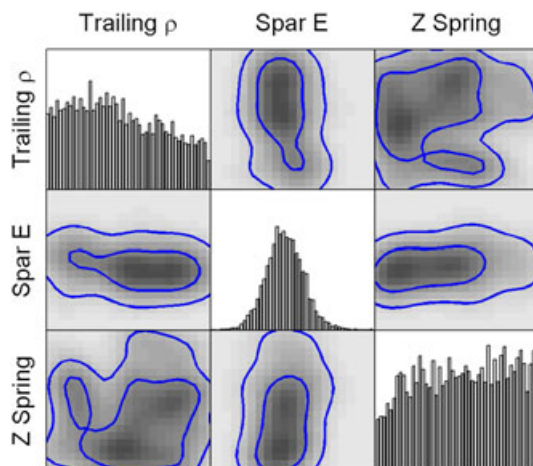


**Figure 10.** Marginal distribution and correlation functions corresponding to Table VII.

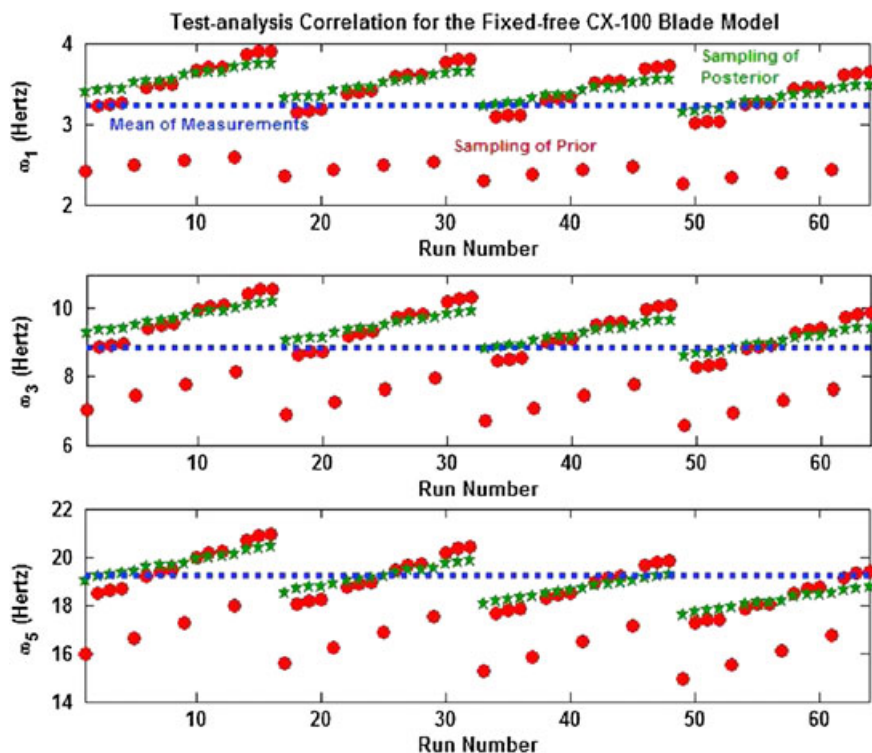


Figure 11. Prior and posterior predictions for the fixed-free configuration.

This application illustrates that the combination of statistical effect screening (Sections 4.2 and 4.4) and inference uncertainty quantification (Sections 4.3 and 4.5) is a powerful tool to reduce the parametric uncertainty of the simplified model. The results obtained answer Question C but prove nothing regarding the predictive power of the model. In Section 5, TAC is applied to the mode shape deflections to assess the overall validity of the model.

## 5. VALIDATION ASSESSMENT USING THE MODE SHAPE DEFLECTIONS

The predictive power of the simplified FE model is assessed through TAC of the mode shape deflections. The reason for this choice is twofold. First, the mode shapes have not been used previously for sensitivity analysis or inference uncertainty quantification. These deflections provide a separate dataset for validation of the model. It is emphasized that using experimental data that were not considered during calibration is essential to validate the predictive capability of a model. One could argue, rightfully so, that the mode shape vectors used for validation are not truly independent from the resonant frequencies used for calibration. After all, they both originate from the same modal test. This is, however, the best that could be achieved given the unavailability of other datasets at the time the study was initiated. The second reason is that the simplified FE model of blade dynamics is developed for a future integration with the simulation of flow around the turbine. For credible fluid-structure interaction, it is important to establish that the model provides accurate predictions of the bending and torsion deflections.

Predictions of mode shapes are generated from multiple simulation runs obtained by sampling the posterior distributions of material properties and spring coefficients for the two boundary conditions considered (both free-free and fixed-free). These runs are used to establish that the simplified model is able to capture several aspects of the problem, such as predicting different attachment conditions or reproducing the overall experimental variability.

The TAC is illustrated graphically in Figure 12 for the free-free boundary condition and in Figure 13 for the fixed-free configuration. In both figures, the experimentally identified mode shapes are plotted using red solid lines. Variability from the simulation predictions is reported with box plots (using blue symbols). The left sides of Figures 12 and 13 compare values of the measured and predicted displacements. The right sides compare the overall deflection shapes of the first three flapwise bending modes.

An excellent degree of correlation is obtained for the first mode shape of the free-free boundary condition in Figure 12; however, the agreement breaks down with higher-order modes. This may be explained by the fact that higher-order mode

shapes are more difficult to excite and identify experimentally. On the modeling side, a higher-order deflection may be more sensitive than the first bending mode to the definition of a relatively small number of sections in the model (only six sections). Both effects would tend to deteriorate the correlation observed. The overall degree of TAC of the first three flapwise bending modes is, nevertheless, deemed satisfactory on the basis of not only these visual comparisons but also the coefficients of correlation estimated next.

Figure 13 illustrates the mode shape correlation for the fixed–free configuration. A high degree of agreement is, again, obtained between the measured and predicted deflections. The higher-order modes tend to be better correlated to measurements than those obtained for the free–free boundary condition. This is a welcomed observation because the simplified model will eventually be integrated to a coupled, structural–fluid simulation of the entire turbine, which implies a fixed attachment at the root of each blade. Less prediction variability is obtained for the fixed–free configuration because only three parameters are varied, compared with the five material properties exercised in the analysis of the free–free boundary condition. The ability of the model to reproduce the experimental measurements, using parameters obtained from an inference based on resonant frequencies, establishes that the boundary springs utilized have the potential to produce reliable predictions of the blade behavior.

The modal assurance criterion (MAC) is calculated to quantify the correlation of mode shapes obtained for the experimental and simulation results. The MAC is a coefficient of correlation:

$$MAC = \frac{(\Phi_{Test}^T \cdot \Phi_{Model})^2}{(\Phi_{Test}^T \cdot \Phi_{Test})(\Phi_{Model}^T \cdot \Phi_{Model})} \tag{1}$$

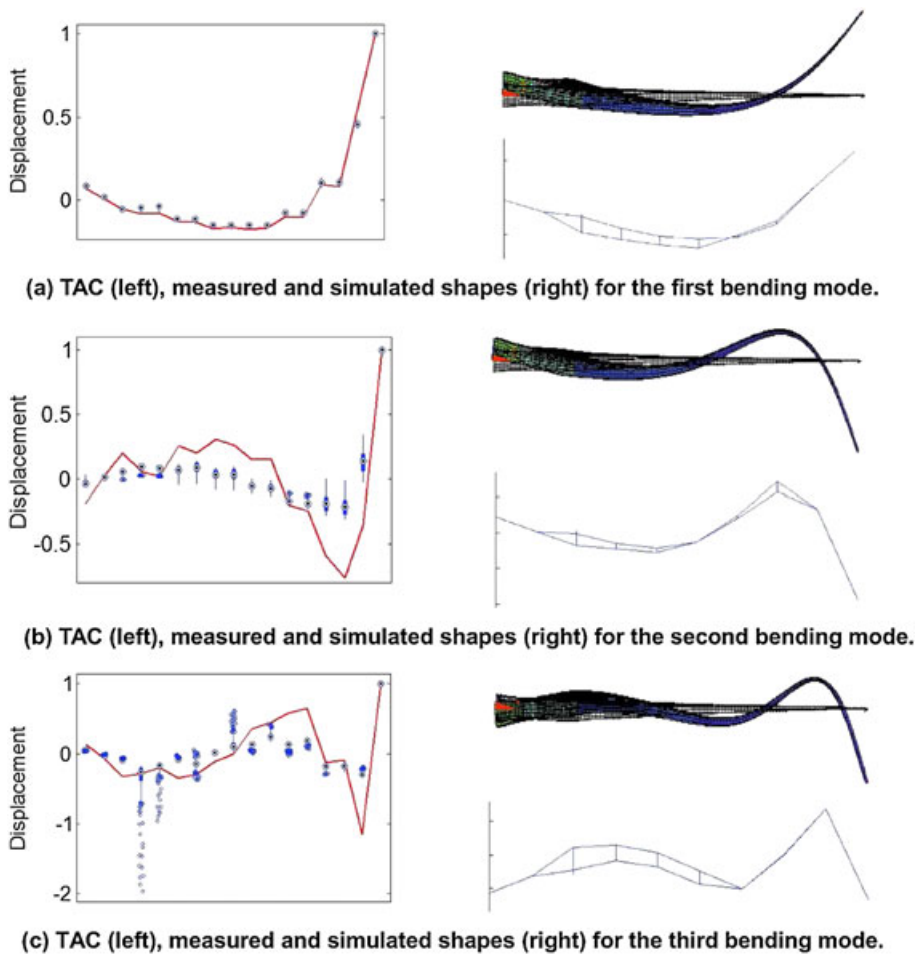


Figure 12. Measured and simulated mode shapes for the free–free configuration.

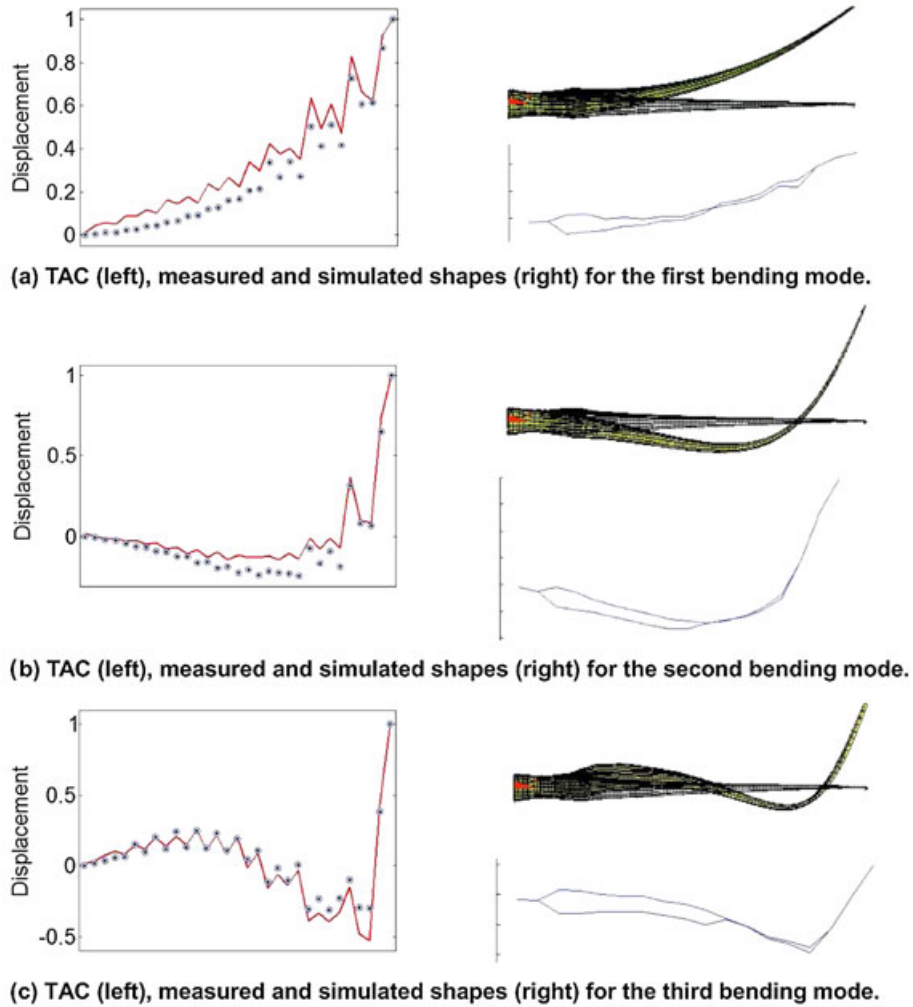


Figure 13. Measured and simulated mode shapes for the fixed-free configuration.

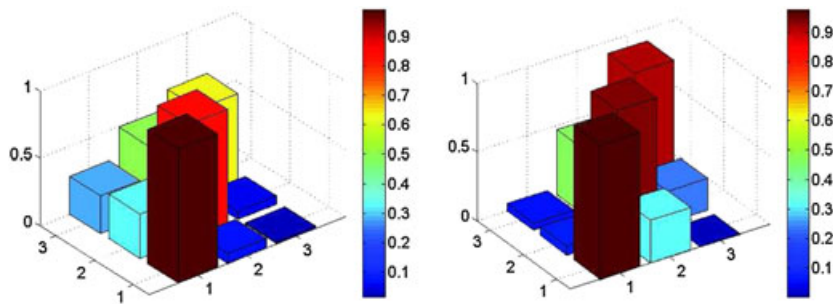


Figure 14. Mode shape MAC of the free-free (left) and fixed-free (right) configurations.

where  $\Phi_{\text{Test}}$  and  $\Phi_{\text{Model}}$  are the measured and simulated mode shapes, respectively, expressed at the same degrees of freedom. The purpose of this analysis is to verify the extent to which the deflections are parallel for the same modes and orthogonal for different modes.

Figure 14 illustrates MAC values for the free-free and fixed-free configurations of the blade. The simulated deflections are predicted by the FE model using average parameter values estimated from the posterior distributions of Figure 4

(free–free) and Figure 10 (fixed–free). Large values on the main diagonal indicate strong correlations between similar modes. On average, the diagonal MAC values are 84% for the free–free boundary and 94% for the fixed–free boundary. Likewise, small values of the off-diagonal suggest that dissimilar modes are orthogonal, as they should be. On average, the off-diagonal MAC values are 21% for the free–free boundary and 19% for the fixed–free boundary. These observations validate the ability of the simplified model to predict mode shape deflections, hence answering Question D.

## 6. CONCLUSION

This second half of a two-part publication discusses the development of a simplified FE model of a wind turbine blade. A particular effort is made to quantify all sources of uncertainty in the simulation and assess their effects on predictions of the low-frequency vibration dynamics of the blade. Because it is exposed to the danger of over-fitting, conventional calibration is not performed to reconcile model predictions and physical measurements. Instead, V&V activities are employed to assess the overall predictive capability of the model. The discussion illustrates what can be learned from specific V&V activities and how these can be integrated to the model development process.

The objective of this work is to develop a fast-running engineering model of blade vibrations for future integration with a fluid dynamics simulation for an entire wind turbine and, eventually, an entire wind plant composed of multiple turbines. It implies that the structural model must be fast-running while providing an accurate-enough representation of the low-order bending and torsion dynamics that will be coupled to the flow around the blade. Four questions are asked regarding specific aspects of the predictive capability being developed.

- **Question A:** What is an appropriate level of mesh resolution for the calculations?

*Answer:* Mesh refinement, combined to an upper bound of solution uncertainty, suggests that a mesh size of 8.0 cm provides accurate-enough predictions of resonant frequencies. The average solution uncertainty, due to truncation error, is estimated to be 1.78%, which is similar to the overall experimental variability (1.62%). This particular mesh, case-specific for our application, provides an extraction of resonant mode shapes and frequencies in less than 60 s. (See Mollineaux *et al.*<sup>12</sup>)

- **Question B:** What are the parameters that most influence the variability of predictions?

*Answer:* DOEs are used in conjunction with variance decomposition to identify parameters of the model that control the variability of frequency predictions. The top three most influential parameters are the moduli of elasticity of the spar cap and leading edge section and density of the trailing edge section. Boundary springs are also influential. Knowing these parameters allows for a more efficient reduction of the prediction variability.

- **Question C:** Can measurements be used to reduce the parametric uncertainty in the model?

*Answer:* Measurements of the vibration response in two configurations, free–free and fixed–free, can be used to reduce the lack of knowledge of model parameters. This is achieved through inference uncertainty quantification, as opposed to deterministic calibration of the parameters. The ignorance of the most influential parameters is reduced by twofold, if not more. The average plus-or-minus one standard deviation statistics are the following:  $E = 40.7 \pm 2.8$  MPa for the spar cap;  $E = 19.5 \pm 5.8$  MPa for the leading edge section;  $\rho = 607.1 \pm 61.4$  kg m<sup>-3</sup> for the trailing edge section; and  $k_2 = 53.7 \pm 27.6$  ( $\times 10^{+6}$ ) N·m<sup>-1</sup> for the boundary springs. Proceeding in two separate steps, first with the free–free blade and then with the fixed–free blade, enables a decoupling between the boundary springs and most other parameters.

- **Question D:** Does the model provide accurate-enough predictions of mode shapes?

*Answer:* The ability of the simplified model to predict mode shape deflections is validated through test-analysis correlation (TAC). The degree of agreement observed is excellent, considering the complexity of the structure, with 84% correlation for the free–free modes and 94% correlation for the fixed–free modes. Datasets used for validation (mode shapes) are kept separate from, and independent of, the data to which the sensitivity analysis and statistical inference are applied (resonant frequencies).

The panoply of V&V activities deployed for this application include verifying the implementation of the software; performing mesh refinements to estimate the solution uncertainty; developing a Phenomena Identification and Ranking Table to define the important parameters; running designs of computer experiments to, first, identify the most significant effects through sensitivity analysis and, second, develop fast-running Gaussian Process Model emulators; propagating uncertainty from model parameters to frequency and mode shape predictions; and performing inference uncertainty quantification to reduce the lack of knowledge of material properties and boundary springs. The overall validation assessment is grounded in the TAC of mode shape deflections, which are data that have not been used for the sensitivity analysis and uncertainty quantification.

The study concludes that our scientific hypothesis is confirmed: a simplified but credible model of the low-frequency, structural response can be developed for future integration with the flow dynamics simulation. This positive finding is an encouragement to pursue this work even further with the on-going development and V&V of a non-linear beam element capable of describing the large displacements and large deformations witnessed by blades during the normal operation

of a wind turbine. Future work will involve integrating the simplified FE model, one-dimensional beam element and computation fluid dynamics software for the numerical simulation of performance of entire wind plants.

The development of future models will also take into account experimental data that further exercise the compliance of the fixed–free boundary condition. New vibration tests have been executed with another suspension system and the addition of masses that further stress the compliance of the fixed–free boundary condition. Future TAC will promote a better understanding of the role that the boundary spring stiffness plays in model development.

## ACKNOWLEDGEMENTS

This work is performed under the auspices of the Laboratory Directed Research and Development project ‘Intelligent Wind Turbines’ at Los Alamos National Laboratory (LANL). The authors are grateful to Curtt Ammerman, project leader, for his support and acknowledge the technical leadership of Gretchen Ellis for the modeling and analysis of wind turbine blades. The authors also wish to express their gratitude to Krystal Deines, Timothy Marinone and Ryan Schultz, students of the 2010 Los Alamos Dynamics Summer School, for supplying the modal analysis measurements of the CX-100 wind turbine blade. LANL is operated by the Los Alamos National Security, LLC for the National Nuclear Security Administration of the US Department of Energy under contract DE-AC52-06NA25396.

## REFERENCES

1. U.S. Department of Energy. 20% Wind Energy by 2030: Increasing Wind Energy’s Contribution to U.S. Electricity Supply. *Report DOE/GO-102008-2567*, Washington, D.C., 2008.
2. Veers PS, Ashwill TD, Sutherland HJ, Laird DL, Lobitz DW, Griffin DA, Mandell JF, Musial WD, Jackson K, Zuteck M, Miravete A, Tsai SW, Richmond JL. Trends in the design, manufacture, and evaluation of wind turbine blades. *Wind Energy* 2003; **6**: 245–259.
3. Ciang CC, Lee JR, Bang HJ. Structural health monitoring for a wind turbine system: a review of damage detection methods. *Measurement Science and Technology* 2008; **19**: 1–20.
4. Liu W, Tang B, Jiang Y. Status and problems of wind turbine structural health monitoring techniques in China. *Renewable Energy* 2010; **35**: 1414–1418.
5. Larsen FM, Sorensen T. New lightning qualification test procedure for large wind turbine blades, *International Conference on Lightning and Static Electricity*, Blackpool, United Kingdom, 2003; 36.1–36.10.
6. Walford CA. Wind turbine reliability: understanding and minimizing wind turbine operation and maintenance costs. *Sandia Report, SAND2006-1100*, Sandia National Laboratories, Albuquerque, NM, 2006.
7. Resor B, Paquette J, Laird D, Griffith DT. An evaluation of wind turbine blade cross section analysis techniques, *52<sup>th</sup> AIAA/ASME/ASCE/AHS/ASC Structures, Structural Dynamics, and Materials Conference*, Orlando, FL, 2010.
8. Jensen FM, Falzon BG, Ankensen J, Stang H. Structural testing and numerical simulation of a 34-m composite wind turbine blade. *Composite Structures* 2006; **76**: 52–61.
9. Freebury G, Musial W. Determining equivalent damage loading for full-scale wind turbine blade fatigue test. *NREL Report, NREL/CP-500-27510*, National Renewable Energy Laboratory, Golden, CO, 2000.
10. Griffith DT, Paquette JA, Carne TG. Development of validated blade structural models, *46<sup>th</sup> AIAA Aerospace Sciences Meeting and Exhibit*, Reno, NV, January 2008.
11. Vermeer LJ, Sorensen JN, Crespo A. Wind turbine wake aerodynamics. *Progress in Aerospace Sciences* 2003; **39**: 467–510.
12. Mollineaux MG, Van Buren KL, Hemez FM. Simulating the dynamics of wind turbine blades: part I, model development and verification, *13<sup>th</sup> AIAA Non-deterministic Approaches Conference*, Denver, CO, April 2010. (Also, Los Alamos report LA-UR-10-5604).
13. Malcolm DJ, Laird DL. Extraction of equivalent beam properties from blade models. *Wind Energy* 2006; **10**: 135–157.
14. Martins M, Perdana A, Ledsam P, Agneholm E, Carlson O. Validation of fixed speed wind turbine dynamic models with measured data. *Renewable Energy* 2007; **32**: 1301–1316.
15. Hemez FM, Ben-Haim Y. The good, the bad, and the ugly of predictive science, *4<sup>th</sup> International Conference on Sensitivity Analysis of Model Output*, Santa Fe, NM, March 2004; 181–193.
16. Griffith DT, Carne TG, Paquette JA. Modal testing for validation of blade models. *Wind Engineering* 2008; **32**: 91–102.
17. Deines K, Marinone T, Schultz R, Farinholt K, Park G. Modal analysis and SHM investigation of CX-100 wind turbine blade. *Rotating Machinery, Structural Health Monitoring, Shock and Vibration* 2011; **5**: 413–438.

18. Griffith DT, Hunter PS, Kelton DW, Carne TG, Paquette JA. Boundary condition considerations for validation of wind turbine blade structural models, *SEM Annual Conference and Exposition on Experimental and Applied Mechanics*, Albuquerque, NM, June 2009.
19. White JR, Adams DE, Rumsey MA. Modal analysis of CX-100 rotor blade and micon 65/13 wind turbine, *28<sup>th</sup> International Modal Analysis Conference*, Jacksonville, FL, February 2010.
20. Bechly ME, Clausen PD. Structural design of a composite wind turbine blade using finite element analysis. *Computers and Structures* 1997; **63**: 639–646.
21. Veers PS, Laird DL, Carne TG, Sagartz MJ. Estimation of uncertain material parameters using modal test data, *36<sup>th</sup> AIAA Aerospace Sciences Meeting*, Reno, NV, Jan 12-15, 1998, AIAA-1998-49.
22. Kong C, Bang J, Sugiyama Y. Structural investigation of composite wind turbine blade considering various load cases and fatigue life. *Energy* 2005; **30**: 2101–2114.
23. Shokrieh MM, Rafiee R. Simulation of fatigue failure in a full composite wind turbine blade. *Composite Structures* 2006; **74**: 332–342.
24. Askeland D, Fulay P, Wright W. *The Science and Engineering of Materials*. CL-Engineering: Stamford, CT, 2010.
25. McKay MD, Beckman RJ, Conover WJ. A comparison of three methods for selecting values of input variables in the analysis of output from a computer code. *Technometrics* 1979; **21**: 239–245.
26. Saltelli A, Chan K, Scott EM. *Sensitivity Analysis*. John Wiley and Sons: New York, NY, 2000.
27. Wilson GE, Boyack BE. The role of the PIRT process in experiments, code development and code applications associated with reactor safety analysis. *Nuclear Engineering and Design* 1998; **186**: 23–37.
28. Kennedy M, O'Hagan A. Predicting the output from a complex computer code when fast approximations are available. *Biometrika* 2000; **87**: 1–13.
29. Higdon D, Gattiker J, Williams B, Rightley M. Computer model calibration using high-dimensional output. *Journal of the American Statistical Association* 2008; **103**: 570–583.